

# SYNTHESIS OF C- DOPED TiO<sub>2</sub> AT VARIOUS DOPING PERCENTAGE FOR UV- VISIBLE LIGHT PHOTO-CATALYSIS

A Dissertation for

PH-651 Dissertation

Credits: 16

Submitted in partial fulfillment of Masters Degree

M.Sc in Physics (Solid State Physics)

Goa University

in the subject of Physics

by

**ABHISHEK GOPAL NAIK**

Seat number: 22P0430021

ABC ID: 999429286169

PRN: 201401708

Under the supervision of

**Dr. RAJESHKUMAR SHANKAR HYAM**

School Of Physical and Applied Science  
Physics discipline



**Goa University**

April 2024



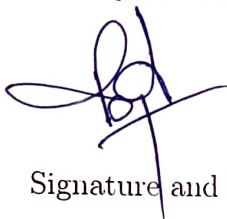
Examined by:

A handwritten signature in blue ink, appearing to be 'R. J.' with a long horizontal stroke.

Seal of the School

COMPLETION CERTIFICATE

This is to certify that the dissertation report "SYNTHESIS OF C- DOPED TiO<sub>2</sub> AT VARIOUS DOPING PERCENTAGE FOR UV- VISIBLE LIGHT PHOTO-CATALYSIS" is a bonafide work carried out by Mr. Abhishek Gopal Naik under my supervision in partial fulfilment of the requirements for the award of the degree of M.Sc in Physics at the School of Physical and Applied Sciences, Goa University.



Signature and Name of Supervisor: Dr. Rajeshkumar Shankar Hyam

Date: 8/5/24



Signature of Dean of the School:

Date: 8/5/24

Place: Goa University



School Stamp

DECLARATION BY STUDENT

I hereby declare that the data presented in this Dissertation / Internship report entitled, "SYNTHESIS OF C- DOPED TiO<sub>2</sub> AT VARIOUS DOPING PERCENTAGE FOR UV-VISIBLE LIGHT PHOTO-CATALYSIS" is based on the results of investigations carried out by me in the Physics Discipline at the School of Physical and Applied Sciences, Goa University under the Supervision of Dr.RAJESHKUMAR SHANKAR HYAM and the same has not been submitted elsewhere for the award of a degree or diploma by me. Further, I understand that Goa University or its authorities will be not be responsible for the correctness of observations / experimental or other findings given the dissertation. I hereby authorize the University authorities to upload this dissertation on the dissertation repository or anywhere else as the UGC regulations demand and make it available to any one as needed.



Name: Mr. Abhishek Gopal Naik

Roll no: 22PO430021

Date: 08/05/2024

Place: Goa University

## ACKNOWLEDGEMENT

I would like thank my guide Mr.RajeshKumar Shankar Hyam as well as Goa University for providing me this golden opportunity to work on this wonderful project on the topic "SYNTHESIS OF C- DOPED TiO<sub>2</sub> AT VARIOUS DOPING PERCENTAGE FOR UV-VISIBLE LIGHT PHOTO-CATALYSIS" which also helped me in doing my research for my project work.

Secondly I would like to thank Miss.Neha Phadte and Miss. Najmeh Hajian Dehkordi for helping me throughout the project and in operating the instruments.

# Contents

<b>1 Introduction</b>	<b>8</b>
1.1 Historical background	8
1.2 Classification of Nano-materials	9
1.2.1 Carbon-based nanomaterials	9
1.2.2 Polymer-based nanomaterials	9
1.2.3 Ceramic-based nanomaterials	9
1.2.4 Metal based nanomaterials	10
1.2.5 Metal-oxide based nanomaterials	10
1.3 Titanium dioxide (TiO <sub>2</sub> )	12
1.3.1 Properties of TiO <sub>2</sub>	12
1.3.2 Applications of TiO <sub>2</sub>	13
1.3.3 Mechanism for photo catalysed dye degradation	15
1.3.4 Carbon (as a Non-metal) doping in TiO <sub>2</sub>	16
<b>2 literature Review</b>	<b>18</b>
<b>3 Experimental technique</b>	<b>21</b>
3.1 Methods available for synthesis of C- doped TiO <sub>2</sub>	21
3.1.1 Ti-C calcination method	21
3.1.2 Template-directed method	22
3.1.3 Hydrothermal Synthesis method	22
3.2 Preparation of sample	24
<b>4 characterisation techniques</b>	<b>26</b>
4.1 X-Ray Diffraction	26
4.2 Raman Spectroscopy	27

<b>4.3 Scanning Electron Microscope(SEM)</b> . . . . .	29
<b>4.4 UV-Vis spectroscopy</b> . . . . .	31
<b>5 Result and Analysis</b>	<b>32</b>
<b>5.1 X-Ray Diffraction Analysis</b> . . . . .	32
<b>5.2 Raman Spectroscopy Analysis</b> . . . . .	34
<b>5.3 Scanning Electron Microscopy(SEM) Analysis</b> . . . . .	36
<b>5.4 UV-VIS Absorption Study of Photocatalytic Degradation</b> . . . . .	38
<b>5.5 Summary</b> . . . . .	39

# List of Figures

1.1 Phases of TiO <sub>2</sub>	12
1.2 Mechanism of photo catalysed dye degradation	15
3.1 Preparation process of porous C-TiO <sub>2</sub> nanostructure.	22
3.2 schematic of an Autoclave	23
3.3 hydrothermal Process	24
3.4 Hydrothermal synthesis of C-doped TiO <sub>2</sub>	25
4.1 Schematic representation of the bragg equation	27
4.2 Schematic representation of Raman spectrometer	28
4.3 Raman scattering and Rayleigh scattering	29
4.4 scanning electron microscope	30
4.5 schematic representation of UV-Vis Spectrometer	31
5.1 XRD data of TiO <sub>2</sub> with 0% doped carbon	32
5.2 XRD data of doped TiO <sub>2</sub> with 1%, 2% and 3% carbon	33
5.3 2 $\theta$ value at (101) of undoped TiO <sub>2</sub>	34
5.4 2 $\theta$ values at (101) of 1%, 2%, 3% doped TiO <sub>2</sub>	34
5.5 Raman spectra of 1%, 2%, 3% C-doped TiO <sub>2</sub>	34
5.6 Raman shifts at 1%, 2%, 3% Carbon	35
5.7 SEM image of (a) 1% C- doped TiO <sub>2</sub> (b)3% C- doped TiO <sub>2</sub>	36
5.8 UV – VIS Absorbance spectrum of (a) 0% doped (b) 1% doped (c) 3% doped	38

# Chapter 1

## Introduction

Nanotechnology is an interdisciplinary field that includes nanoscience investigations on matter ranging from 1-100 nm. Metal Oxide Nano-particles (MONP's) exhibit unique optical, electrical and catalytic properties as compared to bulk materials, which has piqued researcher's curiosity.

### 1.1 Historical background

Nanotechnology is the manipulation of matter at the atomic, molecular, and supramolecular levels (dimensions ranging from 1 to 100 nm) to create new technologies with superior properties. The concept of nanotechnology was introduced by Richard Feynman, the American physicist in 1959. [8] He proposed that it would be feasible to successfully handle and control materials at the atomic and molecular scales for electrical and mechanical systems with nanoscale components. Later Norio Taniguchi, a Japanese physicist, coined the term 'nanotechnology' in 1974 at the International Conference on Production Engineering in Tokyo from August 26 to August 29. He demonstrated the use of semiconductors, such as thin film deposition and Ion beam milling, at a length of 1 nm. He went on to define nanotechnology as the separation, integration, and deformation of materials utilizing only one atom or molecule. [1]

## 1.2 Classification of Nano-materials

### 1.2.1 Carbon-based nanomaterials

Carbon-based nanomaterials typically take the shape of tubes (CNTs) or hollow spheres (fullerenes). These materials are widely employed in electronics, energy storage, industrial catalysis, and nanomedicine due to their distinctive form and high surface area-to-size ratios. Carbon nanomaterials have unique features, including high surface area and outstanding mechanical and electrical properties, making them suitable for therapeutic and diagnostic applications. CNT walls are made up of one or more layers of graphene sheets. Single-walled carbon nanotubes (SWCNTs) are generated by rolling a single graphene sheet, whereas multi-walled carbon nanotubes (MWCNTs) are formed by rolling several graphene sheets. [\[16\]](#)

### 1.2.2 Polymer-based nanomaterials

Other nanoparticles with applications in nanomedicine include polymer-based nanomaterials. Polymers are ideal for structural applications due to their lightweight, easy processing, and long-lasting stability. Polymeric nanocomposites/nanomaterials (PNCs) have gained global interest as a promising technology in a variety of industries. Polymers have advantages in terms of ease of production, corrosion resistance, and low density. However, their strength and stiffness are lower than those used in structural applications. [\[7\]](#)

### 1.2.3 Ceramic-based nanomaterials

Ceramic nanomaterials possess unique features that make them valuable in a variety of applications. Ceramic nanoparticles have high strength and hardness due to their organized crystal structure. Ceramic nanoparticles maintain stability and characteristics at high temperatures, making them ideal for applications including thermal barrier coatings, fuel cells, and catalysis. Their large surface area-to-volume ratio improves their reactivity and interaction with other materials. Nanoparticles with unique optical and magnetic properties like photoluminescence and magnetoresistance, have uses in sensors and data storage. [\[15\]](#)

### 1.2.4 Metal based nanomaterials

Metal-based nanomaterials (MNPs) have been used in a variety of applications due to their unique features. Although they offer distinct advantages, they also have drawbacks related to shape, size, composition, surface area, and charge. They are commonly used as carriers for medicines, biomolecules, and genes in medicinal therapies.<sup>[20]</sup> MNP's have been employed as carrier and contrast agents in imaging, as well as active or passive tumour cell targeting. The creation of these MNPs paves the path for new drug delivery platform for specific targeting, and gene delivery. Gold nanoparticles (Au NPs) are effective gene carriers for cancer treatment due to their high biocompatibility with biomolecules such as nucleic acids. Silver nanoparticles (Ag NPs) have a high gene-binding affinity, making them suitable carriers for gene therapy to treat disorders like cancer. <sup>[16]</sup>

### 1.2.5 Metal-oxide based nanomaterials

The only precursors used to create metal oxide nanoparticles are metals. In many branches of physics, chemistry, and material sciences, these nanoparticles are important. Metal elements are capable of producing a wide range of oxide compounds. These can have a wide range of structural geometries and an electrical structure that can be metallic, semiconductor, or insulator in nature. Metal Oxide Nanomaterial with a configurable band gap, cheap cost, wide specific area and ease of fabrication have attracted a lot of interest in the development of flexible and wearable sensors. Furthermore, metal oxide nanoparticles (MONs) are in high demand in a variety of applications including environmental protection, health monitoring, gas leak alarms, piezoelectric devices, fuel cells, catalysts, and smart device integration with other systems. The transition metal oxides (TMO's), comprised of oxygen atoms bonded to transition metals, are widely used in electronic applications due to their better semiconducting characteristics. Spinal oxides (especially ferrites) exhibit impressive magnetic and electrical properties, making them a promising material for new applications. Zinc oxide NPs (ZnO NPs), cerium oxide NPs (CeO<sub>2</sub> NPs), iron oxide NPs (Fe<sub>2</sub>O<sub>3</sub> NPs), silver oxide NPs (AgO NPs), magnesium oxide NPs (MgO NPs), titanium oxide NPs (TiO<sub>2</sub> NPs), nickel oxide NPs (NiO NPs), zirconium oxide NPs (ZrO NPs) and cadmium oxide NPs (CdO NPs) are the promising examples of metal oxide nanoparticles. <sup>[16]</sup>

### Properties of Metal Oxide nanomaterials

Nanoparticle research is a highly active field with numerous potential applications. Nanoparticles electronic structures can be semiconductor, metallic, or insulator. MONPs have unique chemical and physical properties due to their high density and small surface corners and edges. Metal oxide nanoparticles have potential uses in various disciplines including materials chemistry, medicine, agriculture, information technology, biomedical, optical, electronics, catalysis, environment, energy, and sensing.

Cell parameters have changed as a result of structural changes associated to size in the nanoparticles. For example, in nanoparticles of CuO, ZnO, SnO<sub>2</sub>, AgO, TiO<sub>2</sub>, CeO<sub>2</sub>, MgO, ZrO<sub>2</sub>, etc. As the size of the nanoparticles reduces, more atoms at the surface and interface produce strain or stress and nearby structural disturbances. Magnetic, conductive, chemical, and electrical properties can all be altered by a nanoparticle's exact size. [\[18\]](#)

## 1.3 Titanium dioxide ( $\text{TiO}_2$ )

Titanium dioxide is a metal oxide and an inorganic material. It is made up of one titanium molecule and two oxygen molecules. Titanium is the ninth most common mineral in the earth's mantle and is present in both plants and animals. The octahedral geometry is shared by the three primary dioxides of titanium. Anatase (tetragonal, space group  $I4_1/amd$ ), Rutile (tetragonal, space group  $P4_2/mnm$ ), and Brookite (orthorhombic, space group  $Pbca$ ) are the three major crystal structures of  $\text{TiO}_2$ . Anatase develops at lower temperatures, but Rutile phase forms beyond  $600\text{ }^\circ\text{C}$ . Because the surface Gibbs free energy of the anatase phase is smaller than that of the rutile phase,  $\text{TiO}_2$  nanoparticles tend to nucleate to an anatase phase at a lower synthesis temperature ( $600\text{ }^\circ\text{C}$ ).  $\text{TiO}_2$  is the formula derived from the assembly of these crystal phases as octahedra, where three titanium (IV) cations share six oxygen anions. [3]

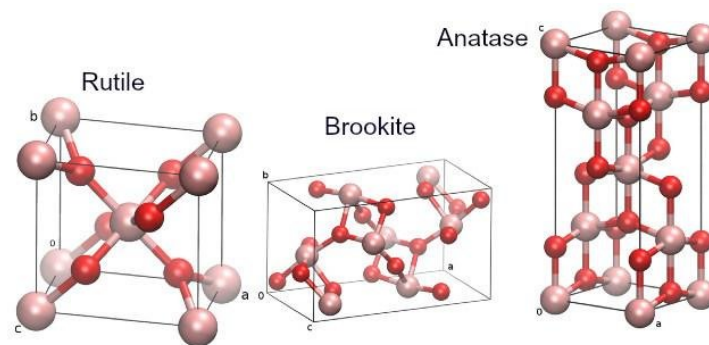


Figure 1.1: Phases of  $\text{TiO}_2$

Titanium dioxide ( $\text{TiO}_2$ ) nanomaterials are well-known for their wide range of uses in both common and advanced products, from sunscreens to photovoltaic cells and a variety of environmental and biomedical applications like drug delivery, water purification, photocatalytic degradation of pollutants, and bio sensing. [19]

### 1.3.1 Properties of $\text{TiO}_2$

#### Optical properties

Rutile is more anisotropic than anatase in the IR to visible spectrum. On the other hand, anatase exhibits significant anisotropy in the band gap area. For rutile, a blue colour appearance that is based on the decrease of  $\text{TiO}_2$ , occurs at around  $0.75$  to  $1.18\text{ eV}$  due

to the visible component of the infrared absorption band peaking. Anatase has also been shown to exhibit the blue colour look in infrared radiation. Additionally, a colour centre at 3.0 eV is caused by an oxygen vacancy that gives a yellow colour. [6]

### Electrical properties

The crystallographic orientations determine the electrical and electronic properties of TiO<sub>2</sub> nanostructures. TiO<sub>2</sub> is a semiconductor with bulk oxygen vacancies, titanium interstitials, and a high resistance of about 1015 Ω cm. These are thought to produce low levels of electron donors that contribute to TiO<sub>2</sub>'s electric conductivity. Photoconductivity is one of the most remarkable electrical characteristics of TiO<sub>2</sub>. When ultraviolet (UV) light surpasses the band gap in energy, electrons become excited and move into the conduction band. As a result, holes—vacancies left by the excited electrons—and mobile electrons are produced, both of which can enhance electrical conductivity. For uses like as photovoltaic cells and photo catalysis, this characteristic is essential. [6]

### 1.3.2 Applications of TiO<sub>2</sub>

#### thin film

Because of its colour and refractive index, it can be deposited as a thin film and is used to create beautiful thin films like "mystic fire topaz" and dielectric mirrors. It is also a highly reflecting optical coating. Alumina, iron oxide, titanium dioxide, and other oxides can be added to certain grades of modified titanium-based pigments to create man-made pigments with glittering, iridescent, and pearlescent effects akin to those of crushed mica or guanine-based products. These pigments are used in sparkly paints, plastics, finishes, and cosmetics. In addition to these effects, a limited colour change may occur in some formulations based on the thickness of the oxide layer in the pigment particle and the way and angle the finished product is illuminated; one or more colours appear through reflection, while the other tones appear as a result of the transparent titanium dioxide layers interfering. [9]

### Sunscreen and UV blocking pigment

TiO<sub>2</sub> is utilized as a thickener, sunscreen, and pigment in cosmetic and skin care products. Ultrafine TiO<sub>2</sub> is utilized as a sunscreen; it is noteworthy because, when paired with ultrafine zinc oxide, it is thought to be a potent sunscreen that reduces the risk of sunburns as well as the immunosuppressive effects, premature photo aging, and photo carcinogenesis linked to prolonged exposure to excessive sun. In general, sunscreens containing compounds like oxybenzone, octocrylene, and octinoxate are thought to be more detrimental to coral reefs than titanium dioxide and zinc oxide. [6]

### Photocatalytic dye treatment

According to Konstantinou and Albanis, one of the biggest categories of hazardous organic compounds consists of textile and industrial dyes. About 15% (one thousand tons) of these non-biodegradable dyes are released into natural streams and aquatic bodies each year through textile waste effluents which are the main sources of water pollution contributing to 17-20%, according to a World Bank estimate. Out of the primary harmful compounds found in wastewater, 72 were only generated during the textile dyeing process, and about 30 of these chemicals could not be treated. TiO<sub>2</sub> has garnered a lot of attention lately for use as a heterogeneous photo catalyst for degrading both atmospheric and aquatic organic contaminants and contributing in environmental purification because of its high Activity. It also demonstrates low toxicity, low pollution load, chemical stability, and affordable availability. In order to boost efficiency, the reactive surface area of TiO<sub>2</sub> has been lowered in size. [9]

### 1.3.3 Mechanism for photo catalysed dye degradation

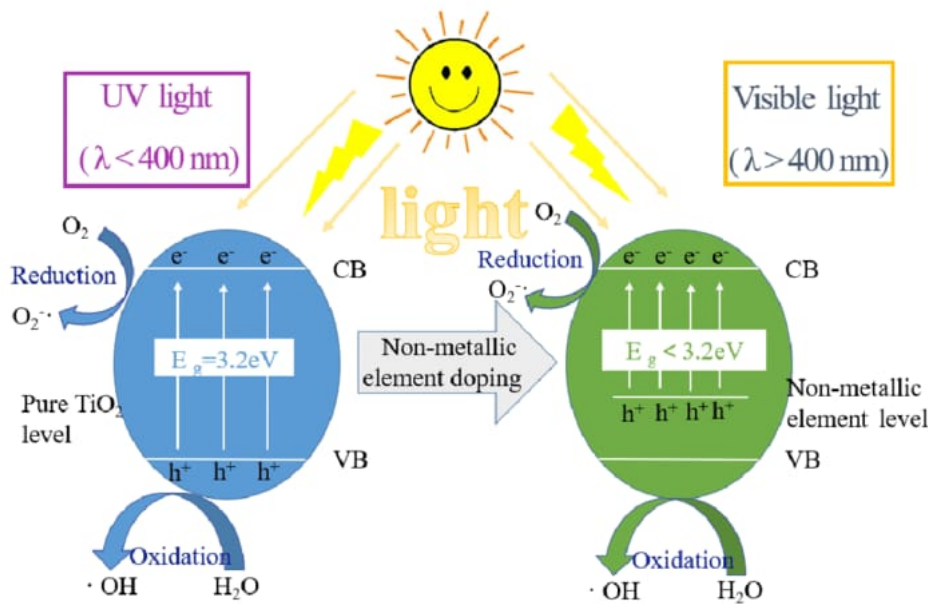
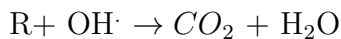
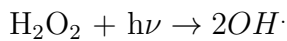
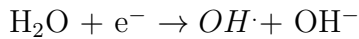
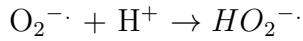
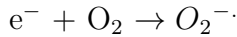
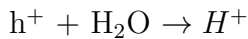
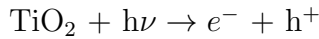


Figure 1.2: Mechanism of photo catalysed dye degradation

A shift of an electron from the valence band to the conduction band results in holes ( $h^+$ ) in the valence band and electrons ( $e^-$ ) in the conduction band when a TiO<sub>2</sub> semiconductor is illuminated with more energy than a band gap. Whereas the holes will interact with the surrounding water to form hydroxyl radicals ( $\text{OH}\cdot$ ), the electrons will interact with the oxygen in the air to produce superoxide radicals ( $\text{O}_2^{\cdot-}$ ).

Both of these free radicals will interact with nearby water-soluble compounds, particularly polymers or organic molecules. The organic component or polymer will break down into carbon dioxide ( $\text{CO}_2$ ) and water ( $\text{H}_2\text{O}$ ) as a result of this hydroxyl radical. Superoxide radicals ( $\text{O}_2^{\cdot-}$ ) will combine with water ( $\text{H}_2\text{O}$ ) to form hydrogen peroxide ( $\text{H}_2\text{O}_2$ ), which will subsequently react with electrons to form hydroxyl radicals. Peroxide will also react with light energy to make hydroxyl radicals ( $\text{OH}\cdot$ ). This hydroxyl radical ( $\text{OH}\cdot$ ) will decompose the organic polymer (R) into water ( $\text{H}_2\text{O}$ ) and carbon dioxide ( $\text{CO}_2$ ).<sup>[9]</sup>

**Reactions involved**

The oxygen deficiency causes it to be an n-type semiconductor in most cases. For anatase, the band gap is 3.2 eV, and for rutile, it is 3.0 eV. Consequently, its wide 3.2 eV band gap means that it can only be absorbed under UV light irradiation (370–415 nm). Even though UV light only occupies up just a small proportion of the solar spectrum (4–5%) it will still be beneficial if we can increase TiO<sub>2</sub>'s photocatalytic efficiency by changing its optical sensitivity to the visible range. Scientists are thus investigating ways to modify TiO<sub>2</sub> in order to enable it absorb visible light.

Most research has focused on doping TiO<sub>2</sub> with transition metals including Cr, Fe, Mn, and V to change its absorption power from the ultraviolet to the visible range. However, due to thermal instability, transition metal doping has poor photocatalytic activity. Thus one of the most effective ways to modify TiO<sub>2</sub>'s photo-absorption characteristics for photocatalysis is the process of utilizing solar light by non-metal doping. [\[9\]](#)

**1.3.4 Carbon (as a Non-metal) doping in TiO<sub>2</sub>**

The crystalline phase of TiO<sub>2</sub> and the technique used to fabricate the carbon-doped TiO<sub>2</sub> nanoparticles determine its photocatalytic activity. The band gap energy of TiO<sub>2</sub> is reduced from 2.96 eV to 2.37 eV due to the carbon atoms doped in C-TiO<sub>2</sub> contributing to the formation of an energy level above the valence band and thus due to its increased photocatalytic performance and lower electron-hole pair recombination, carbon-doped TiO<sub>2</sub> has been interestingly considered as a viable and effective photo catalyst. [\[13\]](#)

Beyond other non-metal doping, carbon doped TiO<sub>2</sub> has promising benefits that can be attributed to the following factors.

1. Carbon holds metallic conductivity.
2. It traps and transports photo-generated electrons, improving the efficiency of photo-induced electron/hole pair separation.
3. When exposed to visible light, carbon can also act as a sensitizer, sensitizing TiO<sub>2</sub>.

This aggregates a lot of thermal energy, facilitates charge transfer from the bulk of TiO<sub>2</sub> into oxidation reaction sites, and further generates a lot of active species. Interestingly, it is always suggested that carbon can penetrate the TiO<sub>2</sub> lattice and replace a lattice O or Ti atom. This leads to the formation of a Ti-C or C-O-Ti bond, which creates a hybrid orbital slightly above the TiO<sub>2</sub>.

### **ABSTRACT**

We report the hydrothermal growth of doped TiO<sub>2</sub> nanoparticles with different concentrations of carbon(1%,2%,3%). The microstructure of the as-synthesized samples is characterized by x-ray diffraction (XRD), Scanning electron microscopy (SEM), Raman spectroscopy to understand the structure and composition and UV-VIS absorption studies are done to understand the photocatalytic degradation of Methyl Orange dye in the presence of UV-Visible light.

# Chapter 2

## literature Review

1) Kashinath A. Bogle et al. synthesized thin films of n-type CdS and PANI (p-type polyaniline) which are surface passivated blue light photodetector. CdS material face passivity and linkage states, chain of PANI are responsible for minimizing the dark current due to which they have a remarkable performance w.r.t rectification and quick response. Surface passivated devices exhibit a drop in the activity of photocurrent during reverse biased, activating the effect of rectification and making them suitable applications for photodetectors. Polaron -II\* transition was seen at around 410nm whereas transition at 850nm via UV-Vis absorption spectra. Band gap of 3.02eV and 1.72 eV indicated the absorption wavelength between LUMO and polaron band. Firmly packed crystallites with good surface morphology was shown by SEM images of thin films of pure CdS. UV and XRD data showed the modification of electrical characteristics of the structures of PANI/CdS, potentially affecting the abilities of photoconductivity of heterostructure devices. [\[5\]](#)

2) S. Karna et al. via hydrothermal method prepared various undoped and doped sodium tantalates( $\text{NaTaO}_3$ ). Doping was done with sulphur and carbon.  $\text{NaTaO}_3$  doped with sulphur exhibited better activity of photocatalysis compared to the undoped  $\text{NaTaO}_3$  and doped  $\text{NaTaO}_3$  with carbon in the methylene blue degradation. Using Tauc plot, the band gaps of all the synthesized compounds were determined. Band gap of s- $\text{NaTaO}_3$  was calculated to be 3.52eV while for c-doped  $\text{NaTaO}_3$  and undoped  $\text{NaTaO}_3$  it was 3.94eV and 3.8 eV, respectively .FTIR spectra of the samples showed some particular peaks. Spectra of  $\text{NaTaO}_3$  showed a prominent band at  $560\text{cm}^{-1}$  indicating stretching bond of

Ta-O. Na-O vibrations showed bands ranging from 1000 to 1630 $\text{cm}^{-1}$ . O-H stretching modes of vibrations resulted in a large peak at around 3400-3500 $\text{cm}^{-1}$ . Carbon doped  $\text{NaTaO}_3$  showed a significant peak at 1068 $\text{cm}^{-1}$  due to  $\text{CO}_3^{2-}$  vibration. Although it was seen that these photo catalysts have a little activity of photocatalysis due to their significant band gap, they did improve the methylene blue solution adsorption. [11]

3) V. L. Chandraboss synthesized carbon doped  $\text{TiO}_2$  using precipitation method which was simple and cost effective. The size range of the nanocomposite was around 40 nm possessing structure spherical in shape. Presence of C, Ti and O in the synthesized composite was confirmed via EDX analysis, indicating carbon particles being enclosed inside the matrix of  $\text{TiO}_2$ . [22]

4) Guanglong Liu et al. prepared thin films of carbon doped  $\text{TiO}_2$  photo catalysts via sol-gel method wherein non-ionizing surfactant was used as template and a carbon source. After 30 minutes of calcination at 400°C, the C- $\text{TiO}_2$  exhibited least photoluminescence (PL) spectra intensity due to the reduced electron and hole pair recombination generated via photolytic source under irradiation of UV light. The rate and ability of photocatalysis of the synthesized C- $\text{TiO}_2$  catalyst was assessed by the degradation of methyl orange under irradiation of visible range light. The highest absorbance of methyl orange was seen at 503nm in acidic state. The photocatalytic activity of the methyl orange degradation was seen to decrease with increasing time of calcination. This may be due to the decrease in the amount of carbon with increasing calcination time. Addition of carbon in  $\text{TiO}_2$  leads to increased decomposition due to lesser crystallite size and reduced energy of the band gap. [4]

5) Ali Akbar Ashkarran et al. synthesized carbon nanotubes, CNT- $\text{TiO}_2$  nanocomposites and  $\text{TiO}_2$  nanoparticles. Preparation was done by simple mixing, simple mixing with heat treatment and also with UV illumination. CNTs and  $\text{TiO}_2$  nanoparticles were synthesized using techniques like arc discharge in water and sol gel preparation method. Nanocomposites of CNT- $\text{TiO}_2$  displayed an effective photocatalytic decomposition of Rhodamine B dye under visible light due to CNT being enclosed in the matrix of  $\text{TiO}_2$ . Absorption of light spectra is broadened by nanocomposites of CNT- $\text{TiO}_2$ . The

efficiency of photocatalysis enhanced significantly when exposed to visible light. It was seen that preparing samples at 80A under UV light resulted in higher activity of photocatalysis degradation than samples of CNT and TiO<sub>2</sub> being prepared by heat treatment and simple mixed. Addition of CNT into TiO<sub>2</sub> improves the activity by capturing electrons that are photo generated and allowing for prolonged separation of charges during exposure under visible light. [2]

# Chapter 3

## Experimental technique

### 3.1 Methods available for synthesis of C- doped TiO<sub>2</sub>

#### 3.1.1 Ti-C calcination method

Titanium carbide has attracted widespread attention due to its excellent properties. This study investigates the process of carbon thermally reducing TiO<sub>2</sub> to prepare TiC through a combination of thermodynamic analysis and experiments. The effects of temperature, TiO<sub>2</sub>/C molar ratio, and time on the phase transformation and morphology evolution of the products are investigated. The synthesis of titanium carbide involves the main reduction path of TiO<sub>2</sub>. A common transition metal carbide is titanium carbide, with a number of desirable characteristics: strong conductivity, low density, high melting point, high hardness (28.5–32 GPa), great elastic modulus, and good corrosion resistance. TiC can be produced when solid carbon and titanium dioxide combine at temperatures between 1700 and 2000 °C for an extended period of time (10–20 hours). The reaction's regulating phase is the carbon's diffusion. Therefore, elevating both the temperature and duration promotes the creation of carbides.<sup>[2]</sup>

TiC has a higher potential for creating C-doped TiO<sub>2</sub> materials through simple calcination due to its rapid charge transfer and strong visible-light absorption efficiency. By calcining TiC in situ, Yang et al. created a C-doped layer on the TiC nanosphere with effective visible light-photocatalytic H<sub>2</sub> generation. Unfortunately, the process of calcining TiC nanoparticles to produce functionalized C-doped TiO<sub>2</sub> with regulated shape, size, and hollow/porous structure is exceedingly challenging. Thus, combining other promising

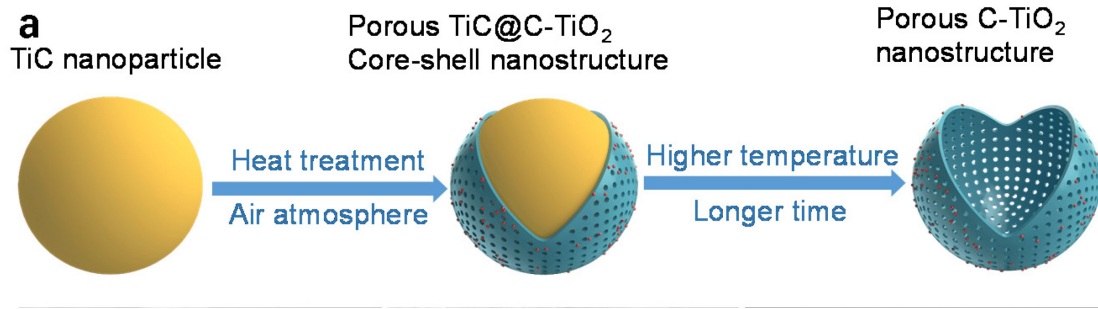


Figure 3.1: Preparation process of porous C-TiO<sub>2</sub> nanostructure.

approaches is crucial to developing C-doped TiO<sub>2</sub> materials with tunable structure and characteristics. [\[10\]](#)

### 3.1.2 Template-directed method

Hollow/porous titanium dioxide nanoparticles are more appealing than solid/nonporous ones due to their larger surface area and numerous interparticle scattering. Since it is a major factor determining their attributes, precise control of the particle size, hollow/porous structure, and shell thickness of TiO<sub>2</sub> spheres has been an objective of research. To create hollow TiO<sub>2</sub> spheres, two basic techniques are introduced in general. One uses a template-free method based on physical phenomena to create hollow TiO<sub>2</sub> spheres.

Another method to solving the drawbacks of the template-free technique is the template-directed method, which successfully adjusts the shell and pore size of hollow TiO<sub>2</sub> spheres. As an example, Zou et al. used carbon spheres as a template to create C-doped hollow TiO<sub>2</sub> spheres. Matos and coworkers described a simple and environmentally benign technique for creating the pristine anatase phase of C-doped TiO<sub>2</sub> by employing a biotemplate made of a molecule produced from biomass. Ji et al. used calcination to create C-doped TiO<sub>2</sub> nanotubes utilizing surface-sulfonated polystyrene as a template. The template-directed method can control the structure of templates to produce a variety of C-doped TiO<sub>2</sub> materials with a regular and tunable morphology at the nano- and/or microscale. [\[10\]](#)

### 3.1.3 Hydrothermal Synthesis method

The process of crystallizing compounds in an aqueous solution at high temperatures and high pressures is known as hydrothermal synthesis. The "hydrothermal method" is another name for technique. Techniques like hydrothermal synthesis, hydrothermal crystal

growth, transformation, sintering, etc others are examples of hydrothermal processing. Nanomaterials processed hydrothermally produce extremely pure, uniform, symmetrical crystal formations with unique characteristics. In addition, it enables dense compounds, low temperature synthesis, increased control over the final product's composition, and the ability to create compounds quickly. [23]

Producing nanocrystalline inorganic materials by hydrothermal processing is an unconventional approach. Since there is a direct precursor-product interaction, almost any substance can be synthesized without the need for agents that define its structure. It is widely recognized that at high temperatures and high pressures, most inorganic materials dissolve in water. This is the foundation of the hydrothermal process, which dissolves the components in water at high pressure and temperature. The desired final products are then obtained by crystallizing these dissolved components.

The process of hydrothermal processing is often carried out in a steel pressure vessel, also known as an autoclave, where the parameters used for processing are controlled through temperature and/or pressure modifications. Teflon coatings for protection may or may not be applied to the autoclave. The procedure is carried out using an aqueous solution. The temperature is raised above the point at which water boils, reaching the saturation pressure of vapor. The amount of solution added to the reaction chamber and temperature have a significant impact on internal pressure (autoclave). In the ceramics sector, this process is often employed to produce minute particles. [24]

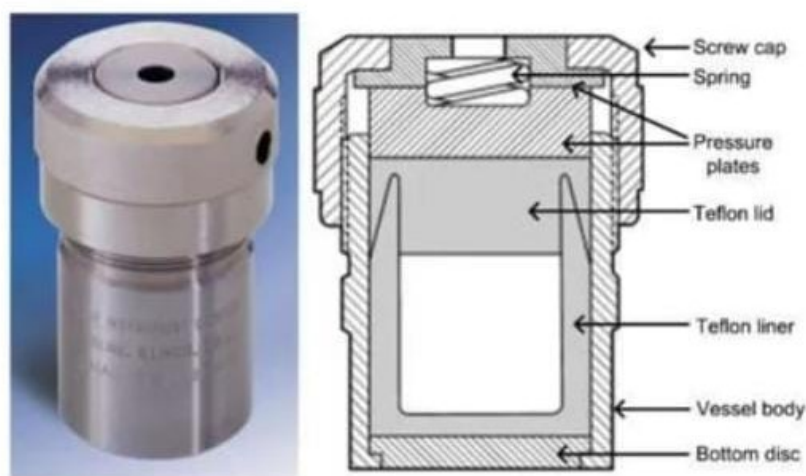


Figure 3.2: schematic of an Autoclave

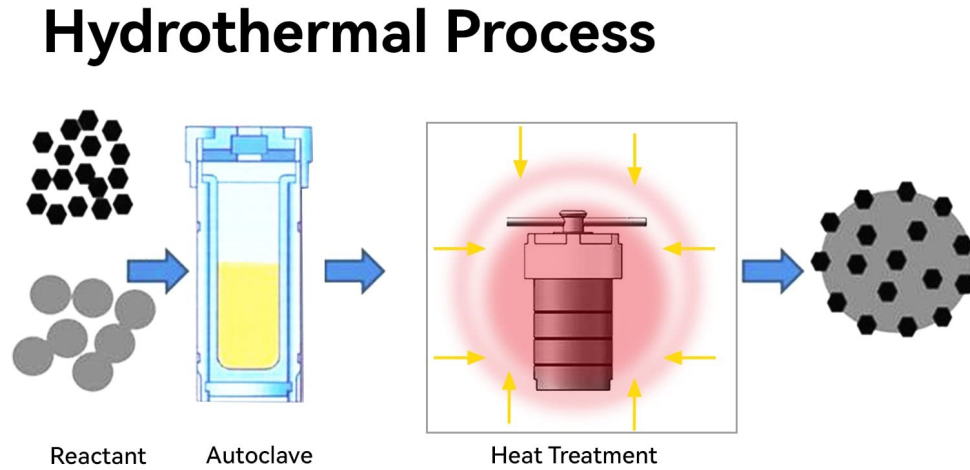


Figure 3.3: hydrothermal Process

Because the hydrothermal conditions can be easily adjusted to influence the morphology and structure of the products, the hydrothermal approach has been widely employed to manufacture C-doped  $\text{TiO}_2$  materials. An acidic or alkaline solution is used to scatter or dissolve the  $\text{TiO}_2$  precursor and carbon source in a conventional hydrothermal synthesis. The mixture is then put into a Teflon-lined autoclave, sealed, and heated in an electric oven (180–200 °C) to create crystalline C- $\text{TiO}_2$  structure. The effective synthesis of C-doped  $\text{TiO}_2$  involves the removal of organic residues using calcination in an airtight atmosphere. [\[24\]](#)

## 3.2 Preparation of sample

The chemicals used for synthesis of Carbon-doped  $\text{TiO}_2$  are Commercial  $\text{TiO}_2$  powder (Mol.Wt. 79.90), Activated Charcoal (M.B. value 220).

Without any kind of treatment, activated carbon and commercial titanium oxide (P25) were used. To ensure excellent homogeneity, a 100 ml of aqueous slurry in DI water containing 0.01 gm of AC and 1 gm of P25 was first sonicated for 30 minutes. It was then autoclaved in a hydrothermal reactor or oven at 200°C for 24 hours. The Autoclave was then left for cooling in the reactor for about 9 hours. The final mixture was then centrifuged, and the solid residue was repeatedly washed with DI water until the filtrate was clear.

In order to optimize the amount of inorganic oxide, the following samples were made: 0.99, 1.96, 2.91 weight% AC in relation to  $\text{TiO}_2$ . In other words, the initial mixtures contains 10 mg (1%), 20 mg (2%), 30 mg (3%) of activated carbon.

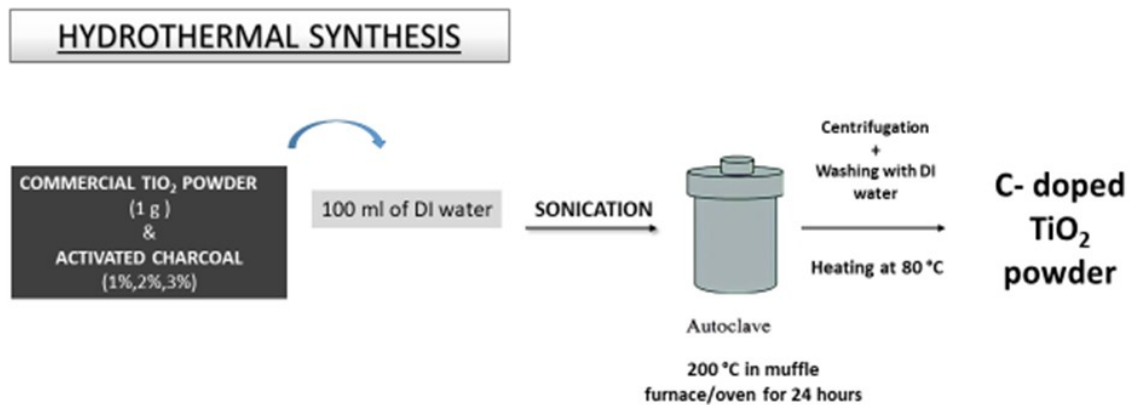


Figure 3.4: Hydrothermal synthesis of C-doped  $\text{TiO}_2$

# Chapter 4

## characterisation techniques

The branch of nanometrology known as "nanoparticle characterization" is concerned with measuring and characterizing the chemical and physical characteristics of nanoparticles. Nanoparticles are frequently developed for their unique properties and have at least one beyond size of fewer than 100 nanometers. Unlike conventional chemicals, nanoparticles possess a variety of physical features comprising size, shape, crystallinity, and dispersion state, making their chemical composition and concentration inadequate for a comprehensive description.

### 4.1 X-Ray Diffraction

By measuring the angles and intensities of diffracted beams of X-rays interacting with a material, X-Ray Diffraction (XRD) is a powerful analytical technique used to characterize the atomic and molecular structure of a crystal. Consequently, XRD can provide detailed information about the crystallography, chemical composition, and physical properties of a material. This article explores the definition, principle of operation, key features, and applications of XRD, mirroring the style and formatting of the excerpts provided. The sample's scattered X-rays can interfere with each other in a constructive or detrimental way. This means that only at angles where constructive interference occurs may detectors read out a signal. The following image shows this schematically.

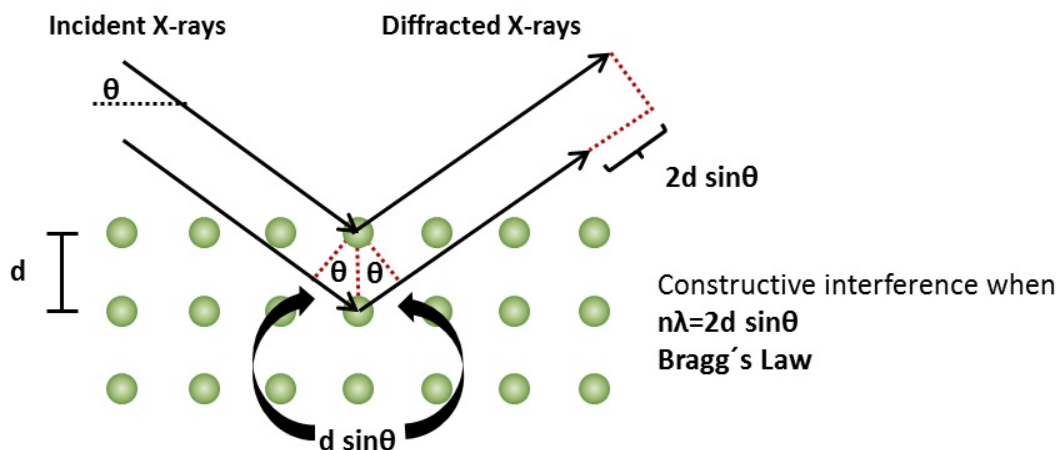


Figure 4.1: Schematic representation of the bragg equation

The graph's dots represent the constituent parts of crystalline materials. Because it is crystalline, the atoms are grouped in a regular pattern. The incident X-ray beam scatters over the material's planes. As a result, the optical path length for the diffracted X-rays to traverse is varied. The X-ray beam's incidence angle and the separation between the crystal planes are the only factors that affect how long the path will be. This satisfies the Bragg- Equation just when the path difference, as determined by  $2d \sin \theta$ , is a multiple ( $n=1,2,..$ ) of the X-ray beam's utilized wavelength does constructive interference take place. The Bragg equation can be used to calculate the separation between the material's lattice planes since the wavelength in XRD experiments is known and the angles at which constructive interference occurs are observed. [25]

A measurement's result is known as a diffractogram. The X-ray intensity is plotted on the y-axis, while the angle  $2\theta$  (which represents the angle between the incident and diffracted beam) is plotted on the x-axis.

## 4.2 Raman Spectroscopy

The analytical method known as Raman spectroscopy uses scattered light to measure the sample's vibrational energy modes. This method offers information on the material's structural and chemical properties in addition to substance identification. Information is extracted from the sample by Raman spectroscopy, which detects Raman scattering.

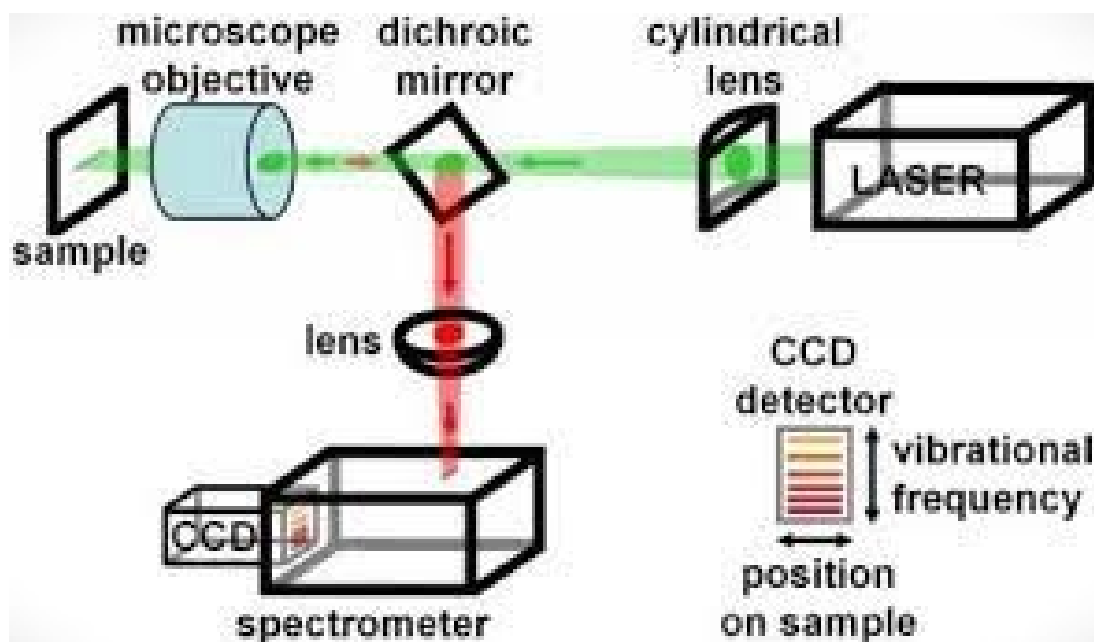


Figure 4.2: Schematic representation of Raman spectrometer

The inelastic scattering of monochromatic light from a laser source, which modifies its frequency upon interaction with the material, provides the basis for the operation of Raman spectroscopy. The Raman effect occurs when laser photons are absorbed by samples and then re-emitted at a frequency that is either higher or lower than the original monochromatic frequency. The rotational, vibrational, and other low-frequency transitions in the molecules are revealed by these frequency shifts. This method is applicable to the investigation of materials that are in the solid, liquid, or gaseous states. Knowing the distinction between Rayleigh and Raman scattering can help us better comprehend spectroscopy. [\[12\]](#)

1. **Rayleigh scattering:** In this case, after the contact with other molecules, the molecules' energy remains constant. The dispersed photons have the same energy and wavelength as the incident photon. Rayleigh scattering is the name given to the phenomenon where the energy of the scattering particle is conserved.
2. **Raman scattering:** In this case, the molecule scatters the light, and the photon's oscillating electromagnetic field causes the molecular electron cloud to polarize, which raises the energy state of the molecules and transfers the photon's energy to them. This can be seen as the creation of the so-called virtual state of molecules. Figure displays the schematic representation of the Rayleigh and Raman scattering. [\[21\]](#)

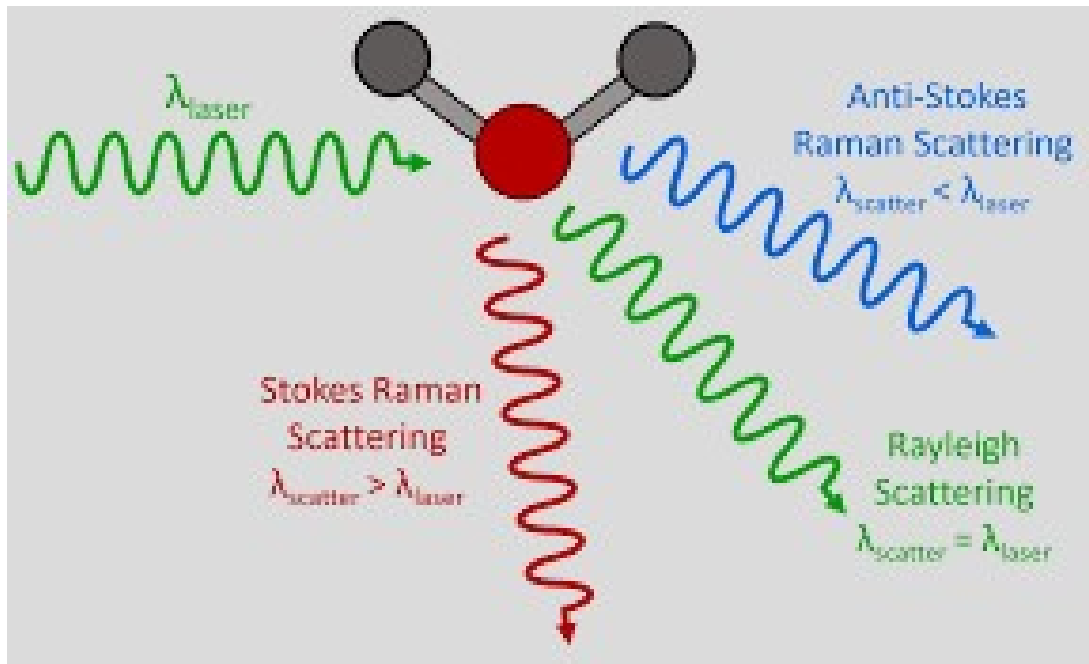
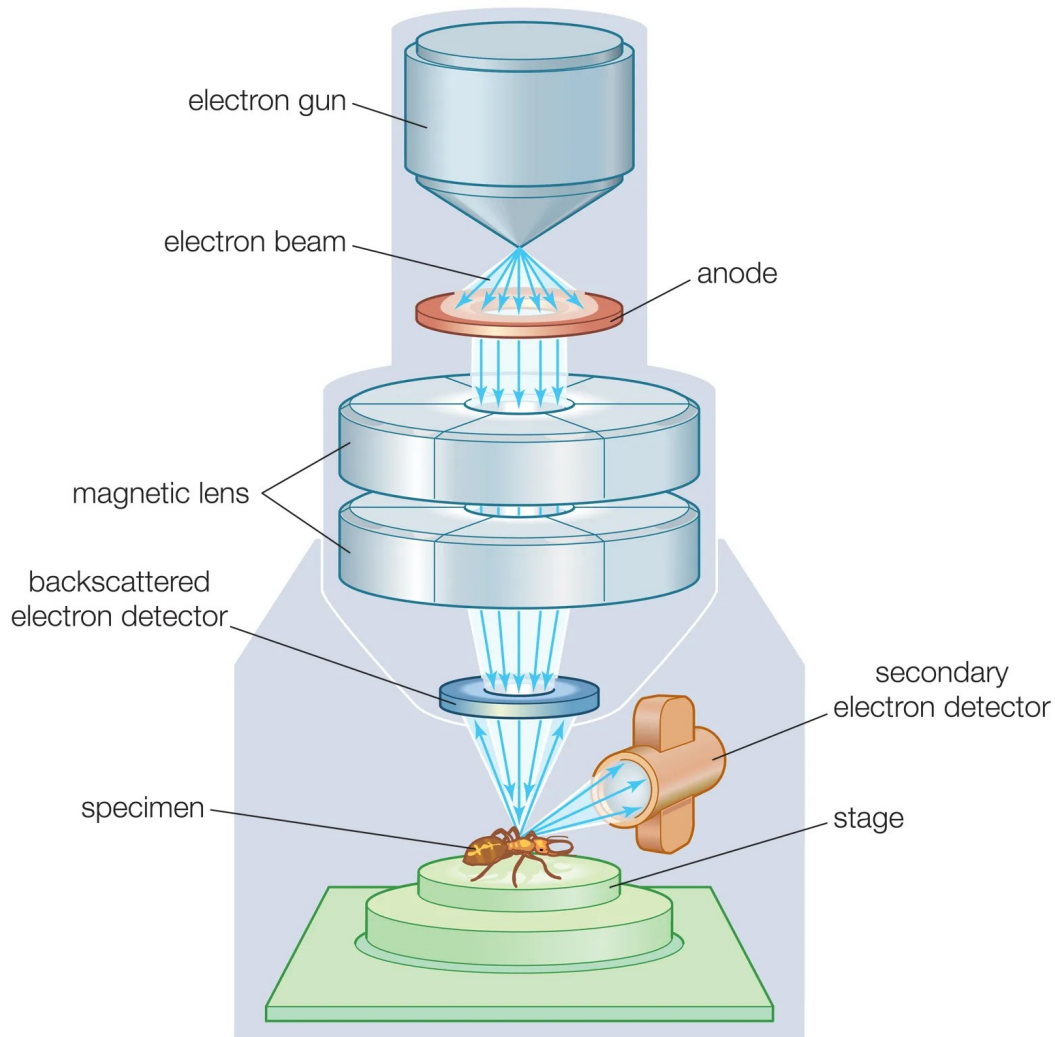


Figure 4.3: Raman scattering and Rayleigh scattering

### 4.3 Scanning Electron Microscope(SEM)

The scanning electron microscope (SEM) is a type of electron microscope used to directly analyze the surfaces of solid objects. It works by scanning a specimen over time with a focused, low-energy electron beam acting as an electron probe. Similar to those mentioned for the transmission electron microscope (TEM), the electron source and electromagnetic lenses that create and concentrate the beam are used in this setup. High-energy backscattered electrons and low-energy secondary electrons are stimulated to emit from the specimen's surface by the action of the electron beam.

Large and bulky specimens may be examined in the SEM without the need for complex specimen preparation procedures. In order to obtain a sharp picture, it is desirable to make the specimen electrically conductive. Typically, conductivity is obtained by vacuum-evaporating a 50–100 angstrom thick layer of metal, such as gold, onto the specimen (this thickness has no discernible impact on the resolution of the surface features). However, nonconducting specimens can be analyzed without the need for a metallic coating if the SEM can run at 1-3 kilovolts of energy.



© 2012 Encyclopædia Britannica, Inc.

Figure 4.4: scanning electron microscope

Focused electron beams are employed by a scanning electron microscope (SEM) to create high-resolution, three-dimensional pictures. These pictures offer details about composition, morphology, and topography. The electron source produces electrons at the top of the column. After that, they are propelled down the vacuum-shielded column, which helps to guarantee high-quality imaging by preventing any atoms or molecules in the column from interacting with the electron beam.

The path of the electrons is altered by electromagnetic lenses. Although the objective lens is primarily responsible for focusing the electron beam onto the sample, the condenser determines the size of the electron beam, which determines the resolution. The beam is projected onto the sample using scanning coils. Apertures are frequently employed together with lenses to control the beam's size. When samples contact with the electron

beam, they release several kinds of electrons. To assist in the detection of backscattered electrons, a Back Scattered Electron (BSE) detector is positioned above the sample. Images can be used to compare locations with differing chemical compositions since areas with higher atomic numbers of heavier elements would seem brighter. To improve the efficiency of detecting secondary electrons, which can provide more precise surface information, a Secondary Electron (SE) detector is positioned at an angle at the side of the electron chamber. [17]

## 4.4 UV-Vis spectroscopy

A scientific method for determining how much light is absorbed or transmitted by a sample at various ultraviolet (UV) and visible (Vis) light wavelengths is called UV Vis spectroscopy. The main focus of ultraviolet-visible (UV-visible) spectroscopy is the absorption of near-UV (180–390 nm) or visible (390–780 nm) radiation by chemical species in solution. This is a quantitative analytical approach. A UV Vis light beam is shined through the sample as part of the procedure, and the amount of light that goes through is measured. Light absorption and transmission patterns can be analyzed to determine and measure the sample's constituent parts. [14]

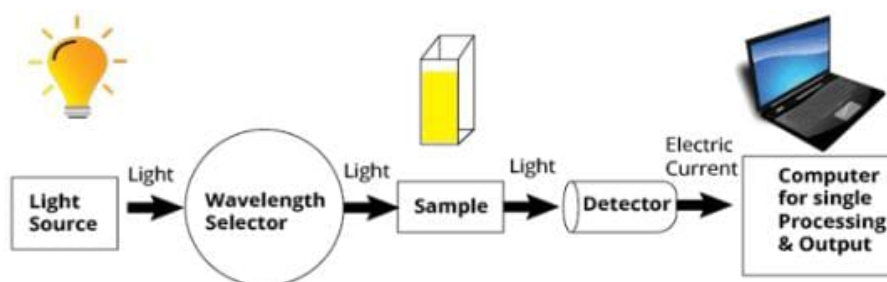


Figure 4.5: schematic representation of UV-Vis Spectrometer

# Chapter 5

## Result and Analysis

### 5.1 X-Ray Diffraction Analysis

The structural properties of undoped  $\text{TiO}_2$  and C-doped  $\text{TiO}_2$  nanocomposites were studied using an X-ray powder diffraction (XRD) analysis, conducted on Rigaku Smart Lab Diffractometer using  $\text{Cu-K}\alpha$  ( $\lambda = 1.5418 \text{ \AA}$ ).

Fig 5.1 shows the X-ray data of bulk undoped  $\text{TiO}_2$  sample, and fig 5.2 shows the x-ry data of all 3 samples that is  $\text{TiO}_2$  doped with 1%, 2%, and 3% of carbon.

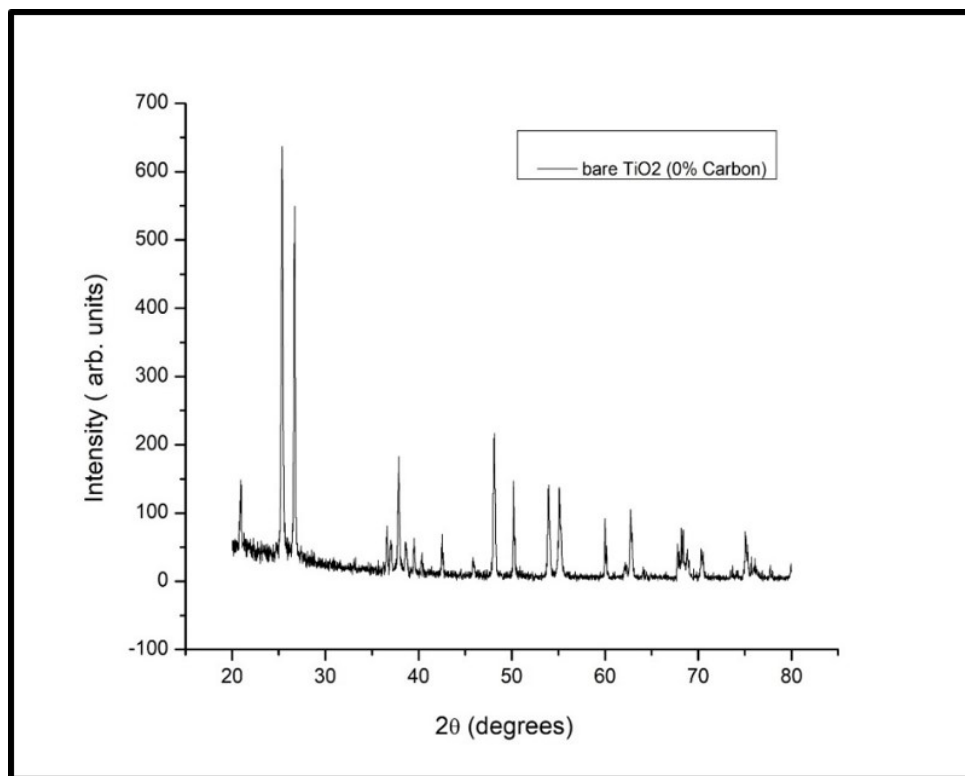


Figure 5.1: XRD data of  $\text{TiO}_2$  with 0% doped carbon

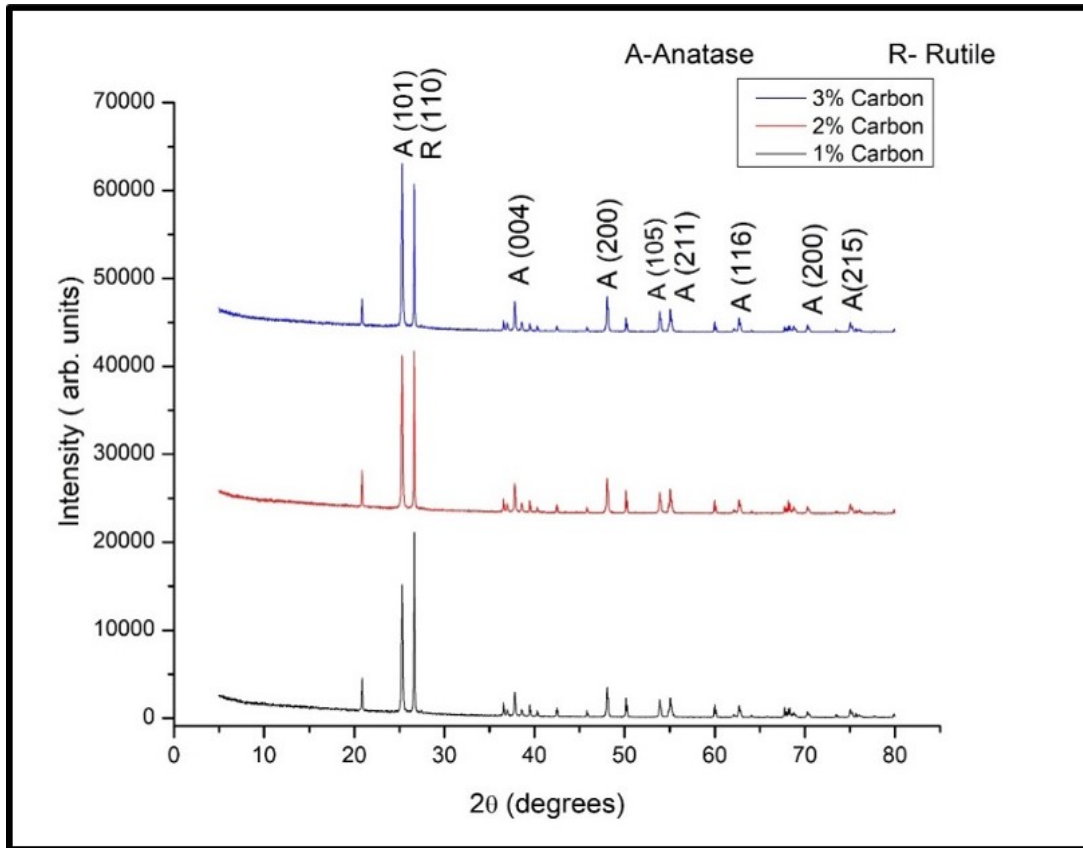


Figure 5.2: XRD data of doped TiO<sub>2</sub> with 1%, 2% and 3% carbon

From the X-Ray diffraction pattern, comparisons of undoped TiO<sub>2</sub> and C-doped TiO<sub>2</sub> samples is analysed and it can be seen that there is increase in intensity with increase in concentration of doping from undoped to 3% doping. It was also observed that there is shift in  $2\theta$  values of titanium oxide peak towards lower value. The delta shift between undoped TiO<sub>2</sub>(0%) with  $2\theta$  value as 25.39 and TiO<sub>2</sub> doped with carbon (3%) with  $2\theta$  value as 25.29 is maximum observed at 0.10 shift for Anatase(101) peak as shown in fig 5.3 and 5.4. XRD shows diffraction patterns of un-reacted carbon of different concentration with both phases that is Anatase and Rutile.

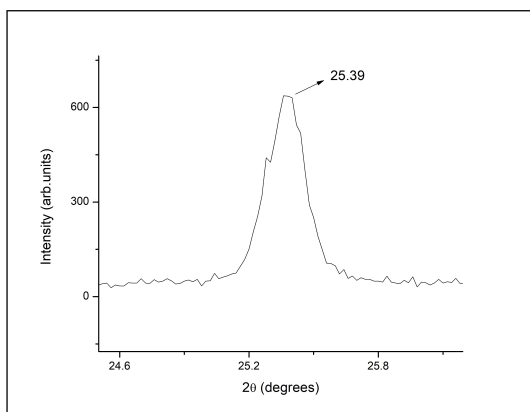


Figure 5.3: 2θ value at (101) of undoped TiO<sub>2</sub>

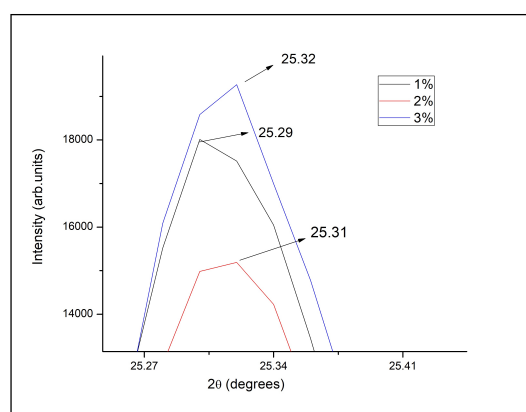


Figure 5.4: 2θ values at (101) of 1%, 2%, 3% doped TiO<sub>2</sub>

## 5.2 Raman Spectroscopy Analysis

Using Raman spectroscopy, the produced materials were studied chemically and vibrationally. The Raman spectra were acquired using a LabRam HR Evolution Raman microscope. By applying a 532 nm laser to the material, the spectra were obtained.

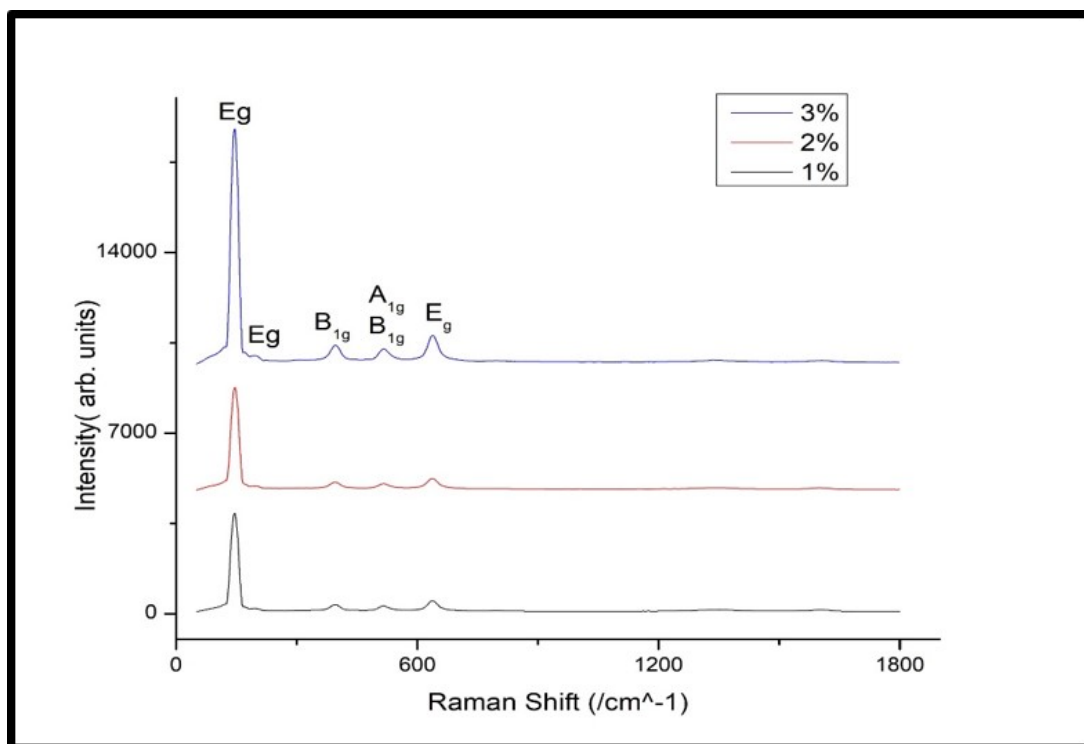


Figure 5.5: Raman spectra of 1%, 2%, 3% C-doped TiO<sub>2</sub>

Raman spectroscopy investigates the vibrational modes of all C-doped TiO<sub>2</sub> NP's. Fig 5.5 shows that there are six active Raman vibrations modes of anatase of TiO<sub>2</sub> as E<sub>g</sub>(145 cm<sup>-1</sup>), E<sub>g</sub>(195 cm<sup>-1</sup>), B<sub>1g</sub>(395 cm<sup>-1</sup>), A<sub>1g</sub>(515 cm<sup>-1</sup>), B<sub>1g</sub>(519 cm<sup>-1</sup>) and E<sub>g</sub>(637 cm<sup>-1</sup>). It is observed that E<sub>g</sub>, B<sub>1g</sub> and A<sub>1g</sub> vibration modes originated from symmetric stretching, symmetric bending and antisymmetric bending vibrations of O-Ti-O in TiO<sub>2</sub> lattice respectively. This is confirmed from the literature.

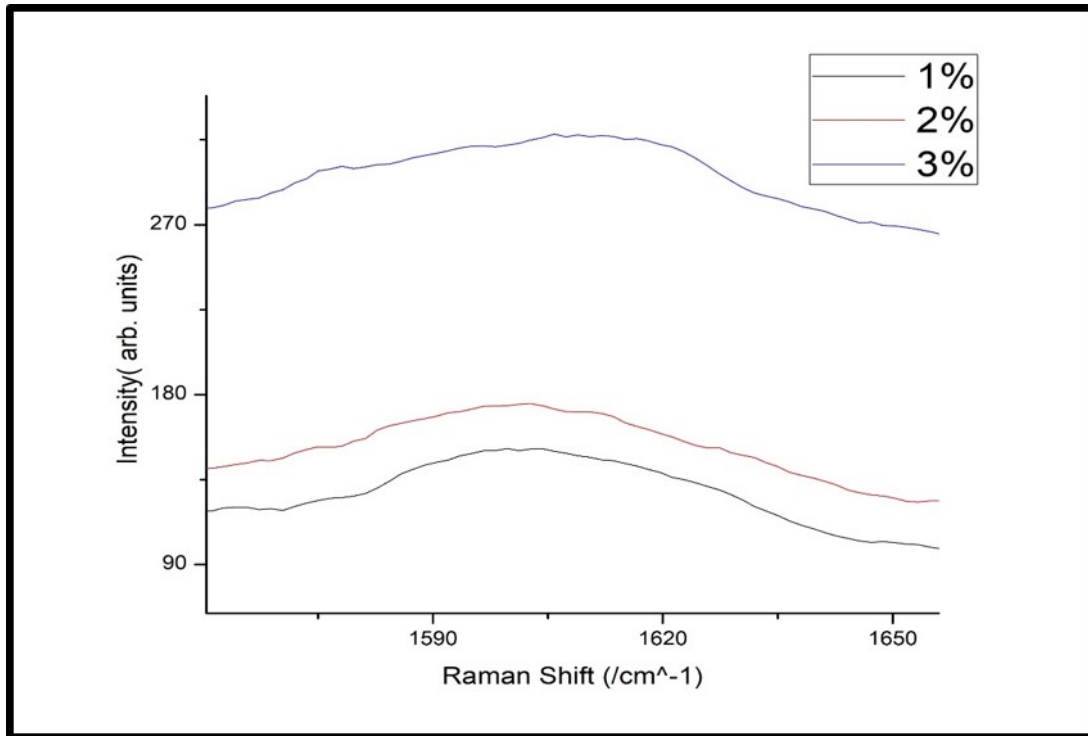


Figure 5.6: Raman shifts at 1%, 2%, 3% Carbon

The intensity of Raman bands increases with increasing concentration. This is may be due to introduction of carbon atoms in TiO<sub>2</sub> lattice, which can cause distortions and defects in the crystal structure. these defects can enhance the cattering of light, leading to stronger Raman signal.

In fig 5.6, peaks observed at Raman Shift of 1599 cm<sup>-1</sup>, 1603 cm<sup>-1</sup>, 1605 cm<sup>-1</sup> as the intensity increases , confirms the Carbon dopant incorporation.

### 5.3 Scanning Electron Microscopy(SEM) Analysis

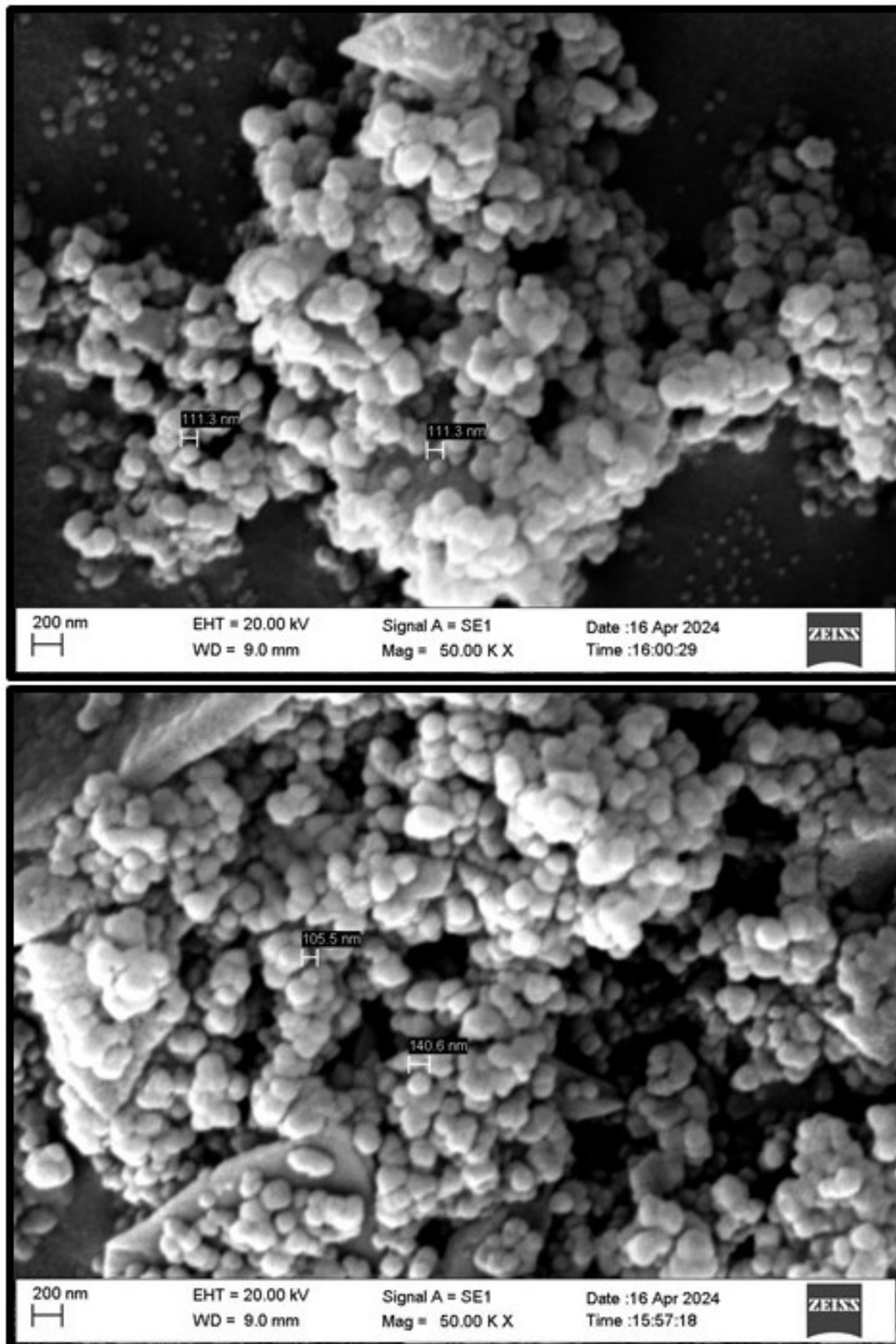


Figure 5.7: SEM image of (a) 1% C- doped TiO<sub>2</sub> (b)3% C- doped TiO<sub>2</sub>

From literature, it is found that SEM data of undoped TiO<sub>2</sub> nanoparticle size show near spherical particles and surface appears to be nearly smooth and relatively defect free. In contrast, samples doped with 1% and 3% (fig 5.7), Carbon appear to have a rougher surface than undoped samples, indicating a change in texture. This may be the result of agglomeration of particles at the surface or decreased crystallinity. Thus it is evident that the morphology of C-doped samples is more homogenous and uniform.

## 5.4 UV-VIS Absorption Study of Photocatalytic Degradation

Testing the prepared samples for photocatalytic applications was the project's main objective. To conduct the photo-degradation experiment, methyl orange was selected. The Lelesil UV-Vis Photochemical Reactor, which used a 250W UV lamp with a dominating wavelength of 280 nm, was used for the experiment. 0.1 mg of Methyl Orange dye solution was prepared in DI water and 50 mg of compound was added, and the mixture was stirred for an hour in the dark to attain adsorption desorption equilibrium before turning on the UV lamp. Using a pipette, 3 ml of this solution were put into a quartz cuvette, and the absorbance spectrum was recorded at 0 minutes before the UV lamp was turned on from 300 and 600 nm using a Shimadzu UV-Vis Spectrophotometer. After the turning on of the UV light, readings were taken at intervals of 20 minutes to 120 minutes. The samples used for experiment are 0% Carbon doped TiO<sub>2</sub>, 1% Carbon doped TiO<sub>2</sub> and 3% Carbon doped TiO<sub>2</sub>

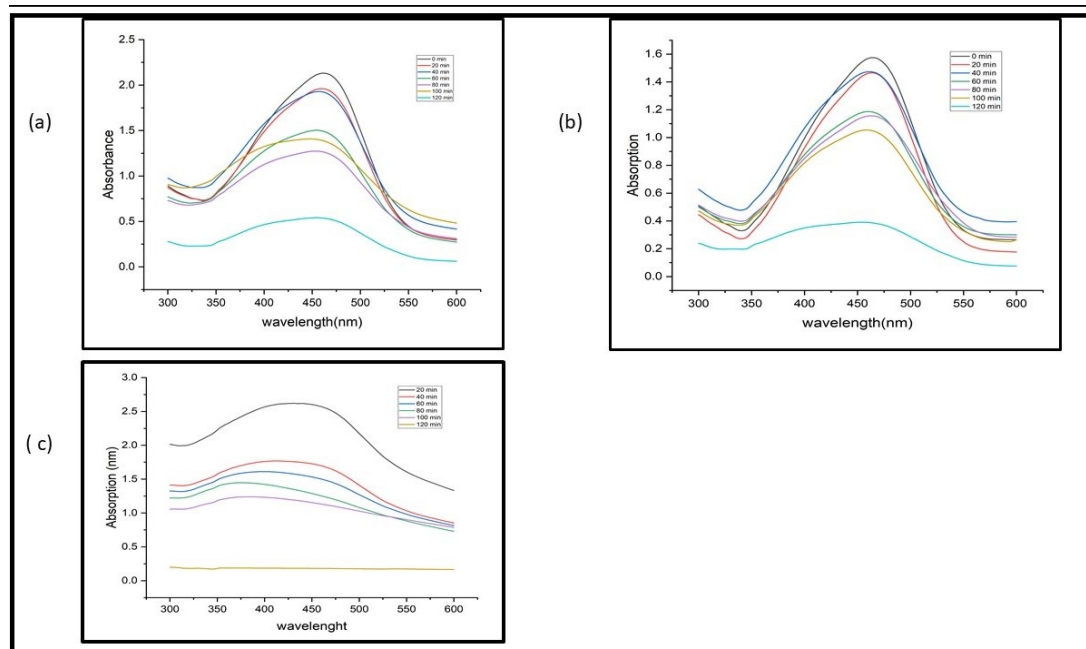


Figure 5.8: UV – VIS Absorbance spectrum of (a) 0% doped (b) 1% doped (c) 3% doped

Carbon doped TiO <sub>2</sub>	0%	1%	3%
Dye Degradation percentage for Methyl orange	74.64 %	75.79 %	92.87 %

Table 5.1: Dye Degradation percentage value for different values of concentration

Percentage degradation formula is given by

$$\% \text{ degradation} = (X_i - X_f / X_i) * 100$$

where  $X_i$  = initial absorbance of dye.

$X_f$  = final absorbance of dye.

It is observed that methyl orange degrades faster in the presence of 3% Carbon doped TiO<sub>2</sub> as the catalyst as compared to undoped TiO<sub>2</sub> as it better photocatalytic degradation percentage. It is also evident that increasing Carbon percentage to an optimum level initiates fastest photoc-catalytic activity.

## 5.5 Summary

Carbon doped TiO<sub>2</sub> nanoparticles were synthesized using a simple hydrothermal process. For the fabrication of C-TNPs, activated carbon were used as carbon source. Under UV-Visible light irradiation, the photocatalytic performance of TNPs and various percent of carbon doped TNPs were examined against Methyl Orange dye. In comparison to bare TNPs, carbon-doped TNPs demonstrated a substantial increase in Visible light-induced degradation which was due to the inclusion of carbon as an “electron and hole trapper” that enables effective charge separation, which is advantageous for photocatalysis. As a result, simple carbon modification allowed the preparation of novel C-TiO<sub>2</sub> Nanocatalysts that have new insights into enhancing the TiO<sub>2</sub>'s photocatalytic performance and have a broad range of environmental applications.

# Bibliography

- [1] Subha Ganguly and SUNIT MUKHOPADHAYAY. “Nano Science and Nanotechnology: Journey from Past to Present and Prospect in Veterinary Science and Medicine”. In: *International Journal of Nanoscience and Nanotechnology (International Research Publication House, Delhi, India)* 2 (Jan. 2011), pp. 79–83.
- [2] Ali Akbar Ashkarran, Majid Fakhari, and Morteza Mahmoudi. “Synthesis of a solar photo and bioactive CNT–TiO<sub>2</sub> nanocatalyst”. In: *RSC Advances* 3 (2013), p. 18529.
- [3] Xiaobo Chen and Annabella Selloni. “Introduction: Titanium Dioxide (TiO<sub>2</sub>) Nanomaterials”. In: *Chem. Rev.* 114.19 (Oct. 2014), pp. 9281–9282.
- [4] Mohamed Hassan et al. “Synthesis and characterization of C-doped TiO<sub>2</sub> thin films for visible-light-induced photocatalytic degradation of methyl orange”. In: *Applied Surface Science* 294 (2014).
- [5] Sandip Patil et al. “Facile synthesis of cadmium sulphide-polyaniline (CdS-PANI) nanocomposite and its field emission investigations”. In: *Journal of Polymer Research* 22 (2015).
- [6] Imran Ali et al. “Recent advances in syntheses, properties and applications of TiO<sub>2</sub> nanostructures”. In: *RSC Adv.* 8 (53 2018), pp. 30125–30147. DOI: [10.1039/C8RA06517A](https://doi.org/10.1039/C8RA06517A). URL: <http://dx.doi.org/10.1039/C8RA06517A>.
- [7] Jinyu Han et al. “Polymer-Based Nanomaterials and Applications for Vaccines and Drugs”. In: *Polymers* 10.1 (2018). ISSN: 2073-4360. DOI: [10.3390/polym10010031](https://doi.org/10.3390/polym10010031). URL: <https://www.mdpi.com/2073-4360/10/1/31>.
- [8] Samer Bayda et al. “The History of Nanoscience and Nanotechnology: From Chemical-Physical Applications to Nanomedicine”. en. In: *Molecules* 25.1 (Dec. 2019).

- [9] Ozioma Akakuru, M Zubair Iqbal, and Aiguo Wu. “TiO<sub>2</sub> Nanoparticles: Properties and Applications”. In: 2020, pp. 1–66.
- [10] Li Hua, Zhengliang Yin, and Shunsheng Cao. “Recent advances in synthesis and applications of carbon-doped TiO<sub>2</sub> nanomaterials”. en. In: *Catalysts* 10.12 (Dec. 2020), p. 1431.
- [11] Sunil Karna et al. “Hydrothermal synthesis of carbon and sulfur mono-doped sodium tantalates”. In: *PeerJ Materials Science* 2 (2020), e10.
- [12] *What is Raman Spectroscopy?* en. <https://www.edinst.com/blog/what-is-raman-spectroscopy/>. Accessed: 2024-5-8. Nov. 2020.
- [13] Cheol Hwan Kwak et al. “Effects of carbon doping on TiO<sub>2</sub> for enhanced visible light-driven NO sensing performance”. English. In: *Materials Letters* 288 (Apr. 2021).
- [14] Justin Tom. *UV-Vis spectroscopy: Principle, strengths and limitations and applications*. en. <https://www.technologynetworks.com/analysis/articles/uv-vis-spectroscopy-principle-strengths-and-limitations-and-applications-349865>. Accessed: 2024-5-8. June 2021.
- [15] Zhimin Gao, Seungjin Lee, and Jiayi Huang. “The Application of Nanoparticle Ceramic Materials in the Design of Modern Handicrafts”. In: *Journal of Nanomaterials* 2022 (June 2022), p. 1998985.
- [16] Yousaf Khan et al. “Classification, Synthetic, and Characterization Approaches to Nanoparticles, and Their Applications in Various Fields of Nanotechnology: A Review”. In: *Catalysts* 12.11 (2022). ISSN: 2073-4344. DOI: [10.3390/catal12111386](https://doi.org/10.3390/catal12111386). URL: <https://www.mdpi.com/2073-4344/12/11/1386>.
- [17] Faith Mokobi. *Scanning electron microscope (SEM)- definition, principle, parts, images*. en. <https://microbenotes.com/scanning-electron-microscope-sem/>. Accessed: 2024-5-8. Mar. 2022.
- [18] Andreea Mariana Negrescu et al. “Metal Oxide Nanoparticles: Review of Synthesis, Characterization and Biological Effects”. In: *Journal of Functional Biomaterials* 13.4 (2022). ISSN: 2079-4983. DOI: [10.3390/jfb13040274](https://doi.org/10.3390/jfb13040274). URL: <https://www.mdpi.com/2079-4983/13/4/274>.

- [19] Anca Diana Racovita. “Titanium dioxide: Structure, impact, and toxicity”. en. In: *Int. J. Environ. Res. Public Health* 19.9 (May 2022), p. 5681.
- [20] Yeosang Yoon et al. “Metal-Oxide Nanomaterials Synthesis and Applications in Flexible and Wearable Sensors”. In: *ACS Nanosci. Au* 2.2 (Apr. 2022), pp. 64–92.
- [21] *Raman scattering: Theory, Raman spectroscopy, and applications*. en. <https://testbook.com/physics/raman-scattering>. Accessed: 2024-5-8. Apr. 2023.
- [22] <https://doi.org/10.26637/MJMOS20/1105>. Accessed: 2024-5-5.
- [23] <http://www.elsevier.com/locate/pcrysgrow>. Accessed: 2024-5-8.
- [24] [https://epgp.inflibnet.ac.in/epgpdata/uploads/epgp\\_content/S000831ME/P001852/M030135/ET/1525855083Module-8\\_unit-3\\_NSNT.pdf](https://epgp.inflibnet.ac.in/epgpdata/uploads/epgp_content/S000831ME/P001852/M030135/ET/1525855083Module-8_unit-3_NSNT.pdf). Accessed: 2024-5-8.
- [25] *X-ray diffraction (XRD)*. en. <https://wiki.anton-paar.com/se-en/x-ray-diffraction-xrd/>. Accessed: 2024-5-8.